A computational study of tandem dual wheel aerodynamics and the effect of fenders and fairings on spray dispersion

By JOHN S. PASCHKEWITZ

Energy and Environment Directorate, Lawrence Livermore National Laboratory, Livermore, CA, 94551

17 January 2006

With the goal of understanding how to mitigate the safety hazard of splash and spray around heavy vehicles, a computational study of the aerodynamics and spray dispersion about a simplified trailer wheel assembly has been completed. A tandem dual slick (TDS) wheel model that neglects complex geometric features such as brakes, wheel bolts and wheel cutouts but with the same dimensions as an actual trailer wheel assembly was used . A detailed simulation of the wheels alone demonstrated that the flow field is both unsteady and complex, containing a number of vortical structures that interact strongly with spray. Preliminary simulations with fenders and fairings demonstrated that these devices prevent the ballistic transport of drops larger than approximately 0.1 mm, but the fine mist speculated to be responsible for visibility reduction is unaffected. This work suggests that to use computational fluid dynamics (CFD) to design and evaluate spray mitigation strategies the jet or sheet breakup processes can be modeled using an array of injectors of small (< 0.01 mm) water droplets; however the choice of size distribution, injection locations, directions and velocities is largely unknown and requires further study. Possible containment strategies would include using flow structures to "focus"particles into regions away from passing cars or surface treatments to capture small drops.

1. Introduction

Splash and spray around heavy vehicles is a longstanding safety problem that has been investigated numerous times over the last thirty years (Weir *et al.* 1978; Manser *et al.* 2003; NHTSA 2000; Allan & Lilley 1983). We define *splash* as the displacement of water in puddles by the tires both toward and outward from the truck and *spray* as very small droplets or mist resulting from the impact of splash or rain on truck or tire surfaces or from aerodynamic or collisional breakup of droplets ejected from the tire treads. The statistical evidence for splash and spray being a significant safety hazard is weak: approximately 20 out of 20,000 accidents were attributed to this problem in the last National Highway Traffic Safety Administration (NHTSA) report to Congress (NHTSA 2000). However, as stated in the NHTSA report (NHTSA 2000), it is possible that accidents due to splash and spray may be attributed to other causes such as driver error and slippery conditions, leading to an underestimate of the problem. Other reports suggest that splash and spray is perceived to be a major problem by the general public. For example, the American Automobile Association (AAA) claims that truck splash and spray is one of the most frequent safety complaints reported by motorists (NHTSA 2000; Manser *et al.* 2003). In response to public opinion, both the state of Oregon (O.D.O.T. 2002) and the European Union have mandated that trucks utilize some form of splash

and spray control. There are a wide variety of aftermarket add-on devices that claim to mitigate the problem, but the experimental test record (Dumas & Lemay 2004; Manser *et al.* 2003; Weir *et al.* 1978; Allan & Lilley 1983; Goering & Kramer 1987*b*,*a*) is rather mixed. Some studies claim that particular fairings or devices are effective while others show the same devices have no measurable impact. Some of the inconsistency in the experimental data reflects the considerable difficulties in obtaining repeatable quantitative measurements of the spray cloud around the truck. Dumas & Lemay (2004) employed SAE recommended practice J2245, which reflects the most current attempt to define a rigorous road test protocol for measuring the spray cloud. This method uses laser-based line-of-sight opacity measurements along the sides of the truck, and Dumas & Lemay (2004) found that even modest crosswinds created large disparities in the data. Given the considerable expense and uncertainty associated with these full-scale tests, it is highly desirable to develop computational approaches to provide insight into whether or not an add-on device is effective.

The impact of truck and wheel aerodynamics on spray cloud formation and transport is less ambiguous than that of any aftermarket add-on devices. The experimental studies of Goering & Kramer (1987*a*,*b*) illustrated that both splash and spray are strongly mitigated by using fully faired wheels. Fully faired wheels are not an operationally acceptable solution since brake cooling and mud or snow fouling are negatively impacted, but these studies clearly illustrate that improving wheel aerodynamics, specifically suppressing the outward wake, has a direct impact on spray transport. Manser *et al.* (2003) examined the effectiveness of a variety of spray suppression add-on devices using both a 1985 and 1997 Freightliner tractor. None of the add-on devices were shown to have a statistically meaningful impact on the spray cloud, but the more streamlined tractor had measurably smaller spray cloud. This result is unsurprising since the width of the spray plume downstream of the truck is heavily dependent on the "bow wave" generated by the tractor and a more streamlined nose will decrease this width.

In this study we consider the interaction between spray and the near-wheel flow field for a simplified trailer wheel assembly. To consider the generation of water droplets by the wheels, it is first necessary to understand the flow about wheel-like geometries. Although the flow around cylinders in various configurations is both numerically and experimentally well-investigated (Zdravkovich 2003), flows around wheel-like geometries have not been examined extensively. The primary source of such studies, which have been completed largely in the last five years, has been meetings of the Society of Automotive Engineers or similar organizations (Knowles *et al.* 2002; Waschle *et al.* 2004; Mears *et al.* 2002; Skea *et al.* 2000; Hedges *et al.* 2002; Basara *et al.* 2000); these studies have largely been experimental and focused on the aerodynamics of open-wheel race cars. The impact of wheel wells (Axon *et al.* 1999) or mudflaps (Elofsson & Bannister 2002) have also been investigated experimentally. There has been only one computational examination of a tandem wheel configuration to the best of our knowledge, which is the study by Hedges *et al.* (2002) of a simplified aircraft landing gear geometry. None of these studies is easily extrapolated to the tandem dual wheel with rotation and ground contact configuration relevant to truck aerodynamics. The primary objective of this study was to obtain preliminary results for the characteristics of the flow around truck wheel geometries in addition to calculating the spray dispersion in the wheel assembly wake.

In this report, simulation results obtained using the commercial computational fluid dynamics (CFD) solver StarCD (cd adapco 2005) are presented. In Section 2, the underlying equations and modeling assumptions used in the spray calculations are presented in addition to the StarCD simulation parameters are discussed. The work presented here has utilized an unsteady Reynolds-Averaged Navier-Stokes (URANS) turbulence modeling

approach combined with empirical correlations for droplet behavior including aerodynamic and collision-induced breakup. In Section 3, we present the details of the wheel simulations. A generic Tandem Dual Slick wheel configuration (or TDS) is considered using a full spray model. Steady RANS results for this same geometry using a fender and a faired fender are also presented; massed particle traces are used in these flow fields to assess the impact of these devices on the spray dispersion. Lastly, our findings are summarized and directions for future research into this problem are discussed.

2. Problem formulation

2.1. *Governing equations for fluid flow*

For both the truck and wheel flow problems we utilize the well-known Reynolds-Averaged Navier-Stokes (RANS) approach in a time-dependent manner. The velocity field is decomposed into mean and fluctuating components Eq.2.1; the resulting *ensemble-averaged* Navier-Stokes equations Eq.2.2 contain an unknown Reynolds stress term that must be defined using a closure approximation.

$$u_i(x_k,t) = U_i(x_k) + u'(x_k,t) \tag{2.1}$$

$$\frac{DU_i}{Dt} = -\frac{1}{\rho}\frac{\partial P}{\partial x_i} + \frac{\partial}{\partial x_j}\left(\nu\frac{\partial U_i}{\partial x_j}\right) + \frac{\partial(\overline{-u_i'u_j'})}{\partial x_j} \tag{2.2}$$

In this work we use the Menter Shear Stress Transport (SST) turbulence model (Menter 1994) to model the Reynolds stresses. This model was chosen since it is implemented in StarCD and has been shown in previous heavy vehicle aerodynamics CFD studies (Salari *et al.* 2004) to be more accurate than the simple $k-\epsilon$ and $k-\omega$ models. This two-equation model is based on the Boussinesq hypothesis that the Reynolds stresses are proportional to the local rate of strain, with the proportionality being the eddy viscosity ν_T:

$$\overline{-u_i'u_j'} = 2\nu_T S_{ij} \tag{2.3}$$

The SST model relates the eddy viscosity to the turbulent kinetic energy k and the turbulence frequency ω:

$$\nu_T = C_\mu k^2/\omega \tag{2.4}$$

Transport equations are solved for both k and ω. By using a weighted average of the $k-\epsilon$ and $k-\omega$ models, with $k-\epsilon$ in the far-field and $k-\omega$ near the wall, the SST model obtains the superior behavior of the $k-\omega$ model near boundaries and for flows with streamwise pressure gradients. This improved performance is obtained while also avoiding the sensitivity of the $k-\omega$ model to the free-stream boundary condition on ω. The default values of the model constants in StarCD correspond to those in the work of Menter (1994).

As is common in commercial code RANS implementations, the "high Reynolds number" turbulence model is coupled to a wall model to compensate for the lack of near-wall resolution in the computational mesh. In the zone below the first grid point away from the wall, the turbulence equations are abandoned and the turbulence and velocity are assumed to follow specified profiles. The wall function thus acts as a boundary condition for the turbulence model at the first grid point off the wall. The wall function approach makes a number of important assumptions: velocity variations are predominantly 1-D and normal to the wall, pressure gradients are negligible and that turbulence production and dissipation are balanced in the wall function zone. Shear stress and velocity are assumed to be aligned and unidirectional in the near-wall region. Given a solution for

the Reynolds-averaged velocity, the skin friction is obtained from the empirical "law of the wall"; the skin friction is then used to obtain a boundary value for k (and ϵ or ω as appropriate). Additional details on wall functions are provided in Wilcox (2002) and Durbin & Reif (2003).

For the fender and faired fender cases, we have used the wall function approach. As these flows have a significant amount of separation, strong curvature, and adverse pressure gradients, we do not anticipate that the resulting wall shear stress predictions will be quantitatively accurate. However, for the preliminary studies performed here that are largely focused on the transport of spray by large-scale flow structures away from the boundaries, we anticipate that our results would not be substantially affected by the use of these wall functions. For the preliminary TDS without fender study we integrated to the wall in the belief that the higher resolution mesh used was adequate; subsequent calculations of the near wall cell spacing demonstrated that this was not the case and a wall function approach is recommended for future simulations.

2.2. *Governing equations for droplet motion*

The droplet motion and breakup are calculated in the Lagrangian frame of reference. This approach requires interpolation of the surrounding carrier fluid velocity onto the center-of-mass of the computational particle representing the droplet. As is common practice in commerical CFD solvers, StarCD uses a "parcel" approach in which each particle represents a collection of droplets with a fixed mass. If the droplets are broken or coalesce, the number of parcels *does not change*; instead the number of droplets represented by the parcel is modified. The one exception to this rule in StarCD is discussed in Section 2.3. The parcel methodology keep the number of particles required to simulate the droplet physics manageable as explicit simulation of the millions of droplets present in even modest atomization problems is not possible due to the enormous computational cost. However, the parcel methodology also underestimates the resulting dispersion of a spray cloud. Lacking a better means of addressing this shortcoming, we used as large a number of parcels as computationally manageable.

The droplet motion in the Lagrangian frame of reference is described by:

$$m_d \frac{d\vec{U_d}}{dt} = \vec{F_d} + \vec{F_p} + \vec{F_{vm}} + \vec{F_b}. \tag{2.5}$$

The aerodynamic drag $\vec{F_d}$ is proportional to the slip velocity of the droplets (which are assumed to be perfectly spherical):

$$\vec{F_d} = \frac{1}{2} C_d \rho_p A_p |\vec{u} - \vec{u_p}| (\vec{u} - \vec{u_p}). \tag{2.6}$$

The effect of local pressure gradients on the particle or droplet motion is given by:

$$\vec{F_p} = -V_d \nabla p. \tag{2.7}$$

In this work, we have chosen to neglect the forces due to "virtual mass" (F_{vm}), which results from the work required to displace the carrier fluid displaced by the drop and buoyancy forces (F_b); scoping simulations in a crossflow atomizer and plane wake including these effects showed minimal differences.

Finally, the backcoupling of particle stresses on the flow field calculation ("two-way" coupling) was not included in this preliminary investigation. The importance of backcoupling can be estimated using a momentum coupling parameter, which is the ratio of

particle drag to the carrier fluid momentum flux:

$$\Pi \approx \frac{C}{1+St}, \tag{2.8}$$

where C is the ratio of the mass flow rates of the disperse and continuous phases and St is the Stokes number, which is the ratio of the response times of the disperse and continuous phases and quantifies the relative importance of particle (disperse phase) inertia:

$$St = \frac{\rho_p d_p^2 U}{18 \mu_c H}, \tag{2.9}$$

where the p and c subscripts denote the particle and continous phases, ρ is the density, d_p is the particle or droplet diameter, U/H is a characteristic flow time scale, and mu_c is the dynamic viscosity (Crowe *et al.* 1998). If this parameter is greater than unity, the backcoupling of particle or droplet momentum on the carrier flow field may be important.

A simple estimate of the importance of the coupling parameter is obtained as follows. Assuming an air flow rate of 20 m/s and a 0.25 m^2 frontal area near the wheel, the mass flow rate is approximately 5 kg/s. The amount of water displaced by the tire patch can be estimated using a tire width (50 cm) multiplied by a tangential velocity (20 m/s) multiplied by a water film thickness (1 mm) to give a mass flow rate of 10 kg/s. This gives a mass loading ratio of 2 in the immediate vicinity of the wheel. For droplets with a diameter of 0.1 mm, the Stokes number is 0.6 using the ratio of the free stream velocity and wheel height (1 m) as the characteristic velocity. These parameters give $\Pi = 1.25$, which suggests that backcoupling is important *near the wheels and for small (low St) droplets*. As the spray disperses away from the wheels, the mass loadings of water strongly decrease and coupling can be ignored; similarly, for very large droplets near the wheels, there is little interaction between the droplets and the flow. Based on these estimates, the smaller droplet behavior near the wheels would be modified if backcoupling were included but that the transport of droplets away from the near wheel region is accurately modeled without these effects included.

2.3. *Empirical relationships for droplet physics*

In this work, we use the most "advanced" empirical models available for the droplet breakup and collision physics in StarCD. For droplet breakup, we use the model of Pilch & Erdman (1987). This model relates experimental observations of various droplet breakup modes to the Weber number, defined as:

$$We = \frac{\rho V^2 D}{\sigma}, \tag{2.10}$$

where ρ is the carrier fluid density, V is the slip velocity between the droplet and the carrier fluid, D is the drop diameter, and σ is the surface tension of the droplet. The Weber number is a ratio of the inertial force, which acts to break the drop, to the stabilizing surface tension force. The second important parameter in the model is the Ohnesorge number:

$$Oh = \frac{\mu_d}{\sqrt{\rho_d D \sigma}}, \tag{2.11}$$

where μ_d is the dynamic viscosity of the droplet liquid, and ρ_d is the droplet density. This parameter is a measure of the importance of droplet fluid viscous to surface tension forces and assumes that the carrier fluid viscosity is small compared to that of the droplet. Pilch & Erdman (1987) curve-fitted data for various breakup modes to ranges of Weber number to derive their model, which allows one to obtain a characteristic time scale for

mode	T	Weber range
Vibrational	$6(We-12)^{-0.25}$	12-18
Bag	$2.45(We-12)^{0.25}$	18-45
Bag-and-stamen	$14.1(We-12)^{-0.25}$	45-351
Sheet stripping	$0.766(We-12)^{0.25}$	351-2670
Wave crest stripping	5.5	> 2670

TABLE 1. Dimensionless total breakup time, T, for droplets as function of Weber number from Pilch & Erdman (1987). Note that the Pilch and Erdman paper has a sign error in the relationship for the bag-and-stamen mode T that is clearly evident upon comparison with their figure illustrating the relationship between T and We.

breakup as well as an estimate for the largest "stable" drop diameter at which no further breakup occurs. Droplet breakup occurs if the Weber number exceeds a "critical" value based on a correlation of experimental data:

$$We_c = 12(1 + 1.077(Oh)^{1.6}) \tag{2.12}$$

If the critical Weber number is exceeded for a given droplet, a dimensionless breakup time, T, based on experimental correlations is obtained and are summarized in Table 1. These correlations assume that the droplet fluid has a low viscosity or $Oh < 0.1$; for water and droplets having a diameter of 1×10^{-3} meters, $Oh \approx 4 \times 10^{-3}$. The breakup time is non-dimensionalized by the ratio $D/(V\epsilon^{0.5})$, where ϵ is the ratio of the continuous to disperse phase densities. This ratio is a time scale obtained using the relative inertia of the two fluids.

The dynamics of drop breakup are then accounted for with several empirical relationships. The maximum stable droplet diameter, D_m, is estimated by noting that the largest stable diameter is the one at which the Weber number equals the critical Weber number with a correction for the fact that as the droplet breaks, the droplet velocity decreases. This correction uses an estimate for the velocity of the droplet "cloud" that results post-breakup:

$$D_m = We_c \frac{\sigma}{\rho V^2} \left(1 - \frac{V}{V_d}\right)^{-2}, \tag{2.13}$$

where V_d is the post-breakup velocity of the droplet cloud. This velocity is obtained using another empirical relationship derived from experimental data:

$$V_d = V\epsilon^{-0.5}(0.375T + 0.2274T^2). \tag{2.14}$$

Finally, the evolution equation for droplet diameter is obtained in StarCD by solving

$$\frac{dD_d}{dt} = -\frac{D - D_m}{\tau_b}, \tag{2.15}$$

where τ_b is the dimensional breakup time constant ($TD\epsilon^{0.5}/V$). We will return to these time scales in the discussion of the droplet breakup behavior in both the tractor-trailer and wheel simulations.

Quantitatively modeling spray impingement on walls is also computationally difficult. We have used the the model of Bai *et al.* (2002) implemented in StarCD to attempt to capture these effects in the simulations presented here. The Bai model was developed to

Mode	modified Weber range
Rebound	$5 < We_d$
Spread	$5 < We_d < 1320La^{-0.18}$
Splash	$We_d > 1320La^{-0.18}$

TABLE 2. Droplet wall impingement regimes from Bai *et al.* (2002).

model the impingement of gasoline spray on engine cylinder walls. The model includes a wide range of droplet-wall collision behaviors: sticking (dry walls only; we assume wetted walls in this work), spreading, rebounding and splashing. The two important non-dimensional numbers in the model are a modified Weber number using the *wall-normal* velocity magnitude, We_d, and the Laplace number,

$$La = \frac{\rho\sigma D}{\mu^2}, \tag{2.16}$$

which characterizes the ratio of inertial to surface tension forces in the droplet. Based on empirical fitting of experimental data, Bai *et al.* (2002) obtained the relationships in Table 2 as a function of modified Weber number. With the impact type determined, the post-impingement characteristics are obtained. For the stick or spread modes, the droplets adhere to the wall; for the latter, the tangential velocity relative to the wall is modified. For a rebound collision, both the normal and tangential velocities are multiplied by an empirical restitution coefficient (which is negative in the case of the wall-normal velocity component) dependent on the incidence angle of the incoming velocity with the wall.

The case of splash is the most interesting: in this case, new computational particles are created (breakup events typically do not lead to this outcome in StarCD's parcel methodology). Two daughter droplets are created and some portion of the original drop remains stuck to the wall. The daughter or secondary parcels represent an equal amount of mass, with the total mass of both determined by an empirical, randomly specified ratio of the total secondary to incident droplet mass ratio:

$$r_s = 0.2 + 0.9X_r, \tag{2.17}$$

where X_r is a uniform deviate random number between 0 and 1. Note that the total secondary mass can exceed the incident droplet mass since the wall is assumed to be wetted and water from the film can be entrained in the daughter droplets. The mass of the fluid remaining stuck to the wall is simply $(1 - r_s)m_d$, where m_d is the mass of the incident droplet (parcel). As each parcel represents a fixed mass of particles, the size and number of droplets in each secondary parcel are calculated using a mass balance and a size randomly selected within an appropriate range defined by the modified Weber and Laplace numbers. Note that StarCD uses an older implementation of the Bai model; the cited reference incorporates size distribution data into this process. Estimates for the secondary droplet ejection angle are obtained by randomly selecting one secondary droplet ejection angle in the range of $5° - 50°$ and then obtaining the remaining daughter droplet angle from conservation of tangential momentum. Lastly, the velocity magnitude is obtained by invoking energy conservation in combination with an experimental size-velocity correlation.

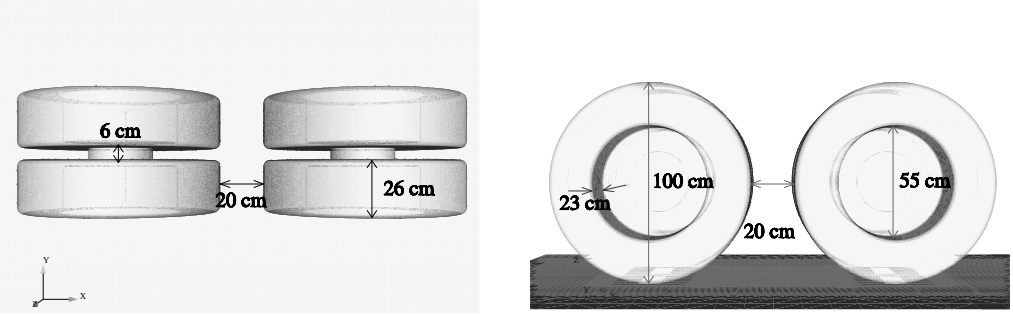

FIGURE 1. Geometry of tandem dual slick model. Left: Top view; Right:Side view

Finally, we note that the effects of droplet coalescence and turbulent dispersion are accounted for in our simulations. The former are modeled using a StarCD-specific implementation that is based on a statistical approach that does not lead to the generation of new parcels; instead the mass and number of droplets represented by a computational parcel is modified if and when collisions occur. The turbulent dispersion model is used to account for the well-known shortcoming that RANS simulations do not account for the interaction of particles or droplets with small flow features, giving rise to erroneous disperion estimates (Apte *et al.* 2003). Using this model attempts to rectify this problem by adding an *ad hoc* random fluctuation velocity proportional to the local turbulent kinetic energy to the droplet velocity, which would otherwise be proportional to the local ensemble average velocity. Finite inertia effects are also accounted for in the response of the droplets to these fluctuations. However, in scoping tests in a cross-flow atomization problem we found that even with this model, droplet dispersion was underestimated.

2.4. *Mesh generation*

To investigate wheel assembly aerodynamics, a simplified geometry we will call the tandem dual slick (TDS) model was generated based on measurements of a trailer wheel assembly. The tandem dual wheels have the correct diameter, overall width, wheel gap, and wheel cutout depth, but the details of the wheel and brake assemblies have been removed. The sidewall curvature has also been ignored and the wheels are approximated as flat cylinders with chamfered edges. The geometric definition is provided in Figure 1.

We have also completed preliminary studies of two additional geometries: the first includes a fender and the second included a faired fender of the Reddaway type found effective in the study of Dumas & Lemay (2004). The fender is similar to the fenders seen on gravel hopper trailers, although for tandem wheels the fenders typically span both wheels and not each individual wheel. We did not attempt to match the fairing size to any real-world configuration since our objective was to qualitatively evaulate the device effect. A simple "mudflap" is also included in the model, but the location and shape of the flap is fixed. A fluid-structure interaction model accounting for the "flapping" of the fender would increase the computational costs significantly and contribute little understanding at this stage of the modeling effort Pictures of the these two spray-reduction device configurations are shown in Figure 2.

These wheel assemblies were meshed the automated meshing tool Harpoon (Sharc 2005). This tool generates boundary layer extrusions without surface wrapping and then transitions these regions to purely cartesian outer meshes. Transitions in mesh resolution can be accomplished using either hanging nodes or tetrahedrals. We have summarized

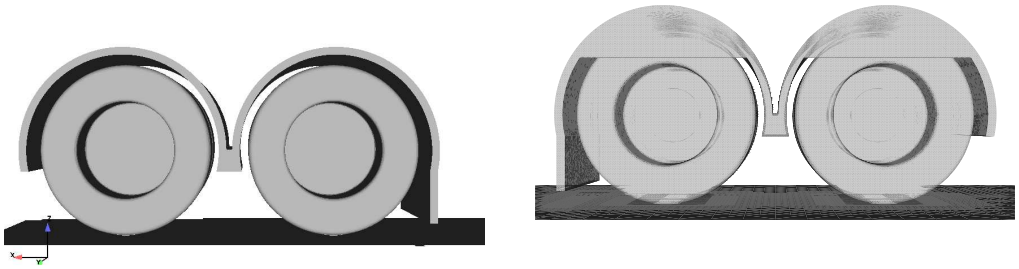

FIGURE 2. Geometry of modified tandem dual slick models. Left: Fender; Right:Reddaway-style fairing. Note the fairings are only on the right side of the fender.

Parameter	Setting
Streamwise domain size (cm)	$-200 < X < 500$
Spanwise domain size (cm)	± 150
Vertical domain size (cm)	$-50 < Z < 200$
Far field mesh size (cm)	12
Surface mesh size (cm)	0.375 (+5 in Harpoon)
Refinement Box (x,y,z,level)	(-85:275;-60:60;-50:90),3.0 (+2)
Refinement Box (x,y,z,level)	(26:95;-35:35;-48:42),1.5 (+3)
Refinement Box (x,y,z,level)	(-70:25;-50:50;-50:50),0.75 (+4)
Boundary layer total thickness (mm)	7.28
Cell size at wall (mm)	2
Boundary layer cell layers	3

TABLE 3. Mesh generation settings used in Harpoon for tandem dual slick (TDS) model. Refinement and resoltion boxes are final, "most refined" values. Slightly coarser settings were used for the fender and faired fender cases

the meshing parameters used in Harpoon in Table 3. Harpoon generates ground contact patches by truncating the geometric object near the ground plane and then creating a "connecting sleeve" with a height equal the user-specified surface cell size. The wheel and sleeve are treated as a single shell cell set by StarCD and the ground plane as a second cell set, making specification of wheel rotation and ground plane motion straightforward. Although Harpoon allows the use of curvature or proximity based surface resolution definition, for this study we have kept the surface cell size constant on all surfaces.

For the baseline TDS model (no fender) we have performed a cursory mesh refinement study to improve resolution of strong gradient regions in the flow. We have found that the front corners of the front wheel, the inter-wheel gap and the wake region all require local refinement regions to adequately resolve the flow. Snapshots of the mesh in the front corner region for each of the the original and refined cases are shown in Figure 3. The final mesh used for the spray dispersion study reported here had approximately 4.5 million cells (with 3 million additional surface cells). The average value of y^+ of the first cell off the wall was appromximately 20 with a maximum of roughly 40 near the contact patch. Since no wall function was used for these simulations, we have underresolved the near-wall region since the first cell should be located at $y^+ < 1$ and the boundary layer

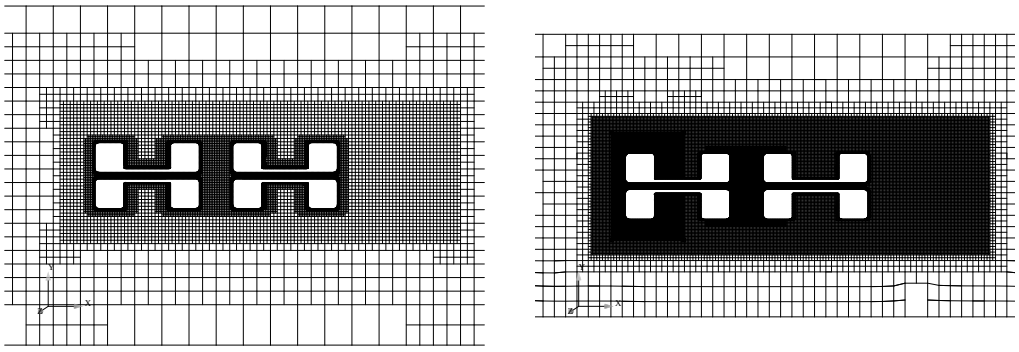

FIGURE 3. Snapshots of mesh for TDS looking from the top down. Left: first attempt at mesh; Right: with refinement in regions of large gradients

should contain roughly 30-40 cells. Future simulations using this mesh should use the wall function, preferably with the adverse pressure gradient option enabled.

2.5. *Problem definition in StarCD*

For the wheel simulations a free stream and moving ground plane velocity of 20 m/s was specified, giving $Re = 1.3 \times 10^6$ based on the wheel diameter. This velocity corresponds to a vehicle velocity of approximately 40 mph. As the transitions between the curved wheel surface and the outer cartesian mesh involve the use of tetrahedral, prism or pyramid elements, the algebraic multigrid solver (AMG) option was used for the pressure solve. The simulations were completed by first obtaining a preliminary flow solution using a steady RANS simulation. This flow field was then used to initialize the URANS simulations; an initial time step of 1×10^{-5} was used and then gradually ramped up to 5×10^{-4} seconds over approximately 500 timesteps and then run for an additional 500 timesteps. Using this final value of the time step, the maximum Courant number was approximately 360 and the mean Courant number was 0.7. The resulting unsteady flow field was then used as an initial condition for the spray study which was run for total simulation time of 0.25 seconds. Runs were performed using 40 processors, taking approximately 100-110 wall clock seconds/timestep. Total simulation time was approximately 150 hours. These statistics make it clear that high-resolution, time-dependent multiphase flow simulations entail a considerably greater computational expense than "simple" aerodynamic calculations.

In the absence of experimental data, reasonable estimates for droplet injection locations and velocities were used. As shown in Figure 4, droplet injection locations were chosen to roughly approximate tire tread locations with injections roughly 45° from the ground plane. To approximate the effect of aerodynamic stripping or "flinging" of small droplets from the thin film of water in the tire treads, an additional set of injection points near the top of the wheel was defined using an initial droplet size of 1×10^{-5} m. A mass flowrate of 5 kg/s was used for each of the droplet sizes ($1 \times 10^{-5}, 1 \times 10^{-4}, 1 \times 10^{-3}$ m) distributed evenly amongst all of the injection points. A total of 300 parcels per injection point (43 injection points in all; 13 for each the larger diameters and the remainder being the 0.01 mm drops) were injected into the computational domain each second.

For the preliminary fender and faired fender cases presented here, only steady RANS runs were completed. The wall function approach was used for these runs since the near-wall resolutions were coarser than those used for the baseline TDS case. No droplet injections were defined in StarCD; instead massed particle traces in the postprocessing program Ensight (CEI 2005) were used to assess the impact of the spray suppression

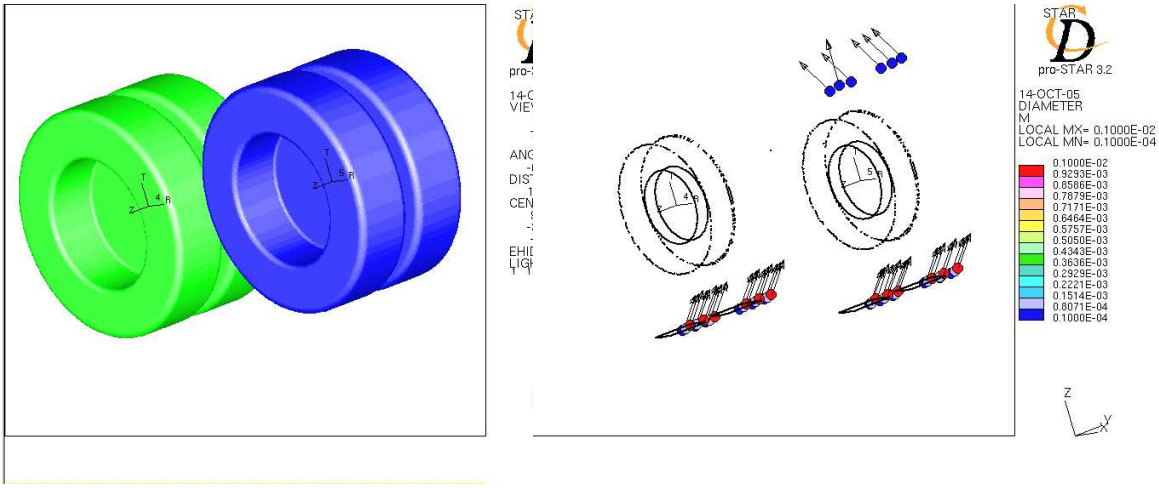

FIGURE 4. (Color) Droplet injection positions and velocity vectors for TDS model. Left:Geometry definition; Right: Cut-away edge plot showing droplet diameters and velocity vectors.

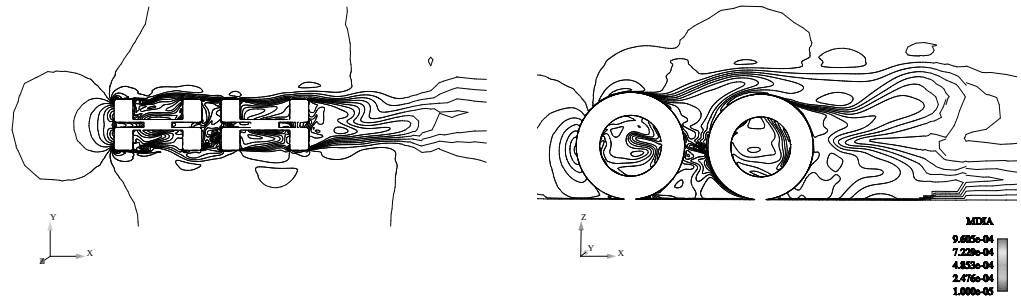

FIGURE 5. Instantaneous visulation of velocity magnitude contours about TDS model. Left: from above at midplane of wheels, Right: from side with cut plane located a center of leftmost wheel

devices. In this case, the massed particles were injected at the local fluid velocity at points roughly corresponding to those in the more rigorous TDS case. Since Ensight's massed particle traces do not include any collisional or aerodynamic breakup models, these results merely illustrate the effect of the devices on trajectories of droplets of various sizes.

3. Results

3.1. *Baseline aerodynamics*

Since there have been no published studies of tandem dual wheel aerodynamics in ground contact to the best of our knowledge, we begin with a discussion of the aerodynamics of this geometry. As shown in Figure 5, the flow about the tandem rotating dual wheels is complex, with a sinuous wake, complex gap flow and separation off the top of the rear wheel at around the 1 o'clock position. There is also strong interaction of the flow with the wheel cutouts.

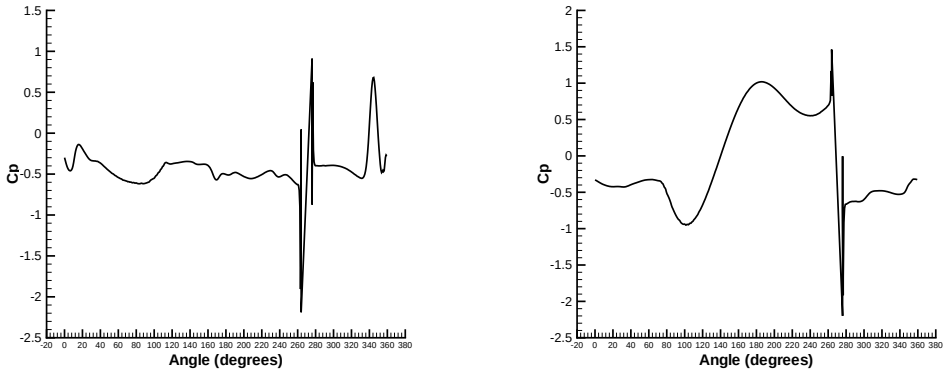

FIGURE 6. Instantaneous pressure coefficient ($C_p = P/(0.5\rho U^2)$) as function of angular position about front (left) and rear (right) wheels in TDS. Pressure profiles obtained at midplane of left wheel in each dual wheel pair. Note that 0 degrees corresponds to the front center edge of the wheel and the angle is defined clockwise from this point.

As might be expected for a bluff body wake, the flow is unsteady and the net forces on the wheels are oscillatory. The time history of the drag coefficient (not shown) suggests a frequency of $\approx 14s^{-1}$; based on a flow timescale of $20s^{-1}$, this would be a Strouhal number of approximately 0.7. For comparison, the study of a dual landing gear by Hedges *et al.* (2002) found that power spectra of URANS simulations showed a comparable Strouhal range of 0.3 to 0.6, with the flow complicated by the presence of the landing gear post.

The most commonly reported data for wheel aerodynamics studies are pressure or C_p profiles. In Figure 6, we present pressure coefficient profile data for the TDS using instantaneous data taken at the end of the run. We anticipate that the time-averaged data will be qualitatively similar, but the reader is warned that considerable variations in C_p are possible in instantaneous data and these results should be considered as preliminary. The angular position is defined with 0 degrees at the front center and clockwise rotation; with this coordinate system the center of the contact patch is at 270 degrees. The C_p profile for the front wheel is consistent with available data (Basara *et al.* 2000; Waschle *et al.* 2004; Mears *et al.* 2002), with large spikes at the contact patch edges due to flow compression and a large C_p at the stagnation point on the front surface. The value of the stagnation point is slightly off-center as observed for rotating wheels by Mears *et al.* (2002), with the maximum value of 0.65 is observed at -15 (345) degrees. The back wheel exhibits substantial differences, with a large low pressure region on the front of the wheel and higher pressure on the back; this result is indicative of the "drafting" effect. This result is consistent with that of Hedges *et al.* (2002).

The coherent structures in the flow are important to the spray dispersion behavior. In Figure 7 we present instantaneous snapshots of the coherent structures in the wake using isosurfaces of the second invariant of the velocity gradient tensor, Q:

$$Q = \frac{1}{2}([tr(\nabla u)]^2 - tr[(\nabla u)^2]), \tag{3.1}$$

where ∇u is the velocity gradient tensor. As shown by Blackburn *et al.* (1996) and Dubief & Delcayre (2000), the isosurfaces of the positive values of Q correspond to regions in the flow where rotation is greater than extension and identify coherent vortex structures. As expected from the literature (Knowles *et al.* 2002; Waschle *et al.* 2004; Mears *et al.* 2002), we see vortex shedding at both the top and bottom of the rear wheel, as well as

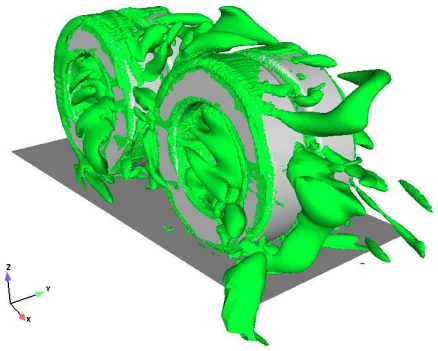

FIGURE 7. (Color) Instantaneous visualization of iso-Q surfaces about TDS. Time=0.155 s, Q level=$1500s^{-2}$

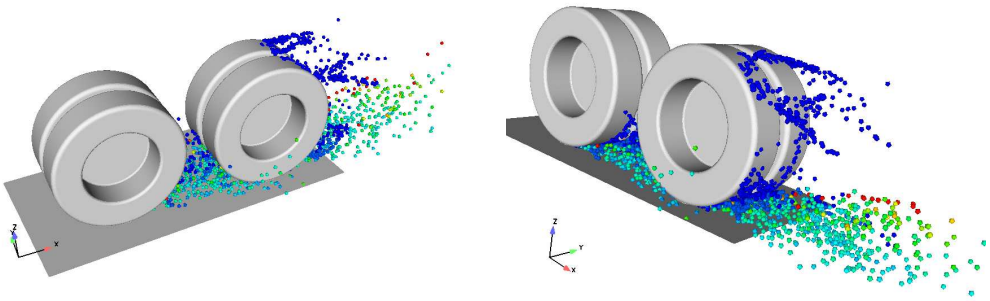

FIGURE 8. (Color) Instantaneous visualization of spray dispersion in TDS wake. Note strong interaction of small (blue) droplets with the coherent structures shown in Fig. 7

from the top of the front wheel. There are actually pairs of counter-rotating vortices, with inwards rotation, along both the top and the bottom of the rear wheel. The pair structure is more clear on the front wheel. These vortex structures interact most strongly with the spray cloud in the wake The wheel cutouts generate large rotational regions that "spill" out of the cavities and into the flow. These structures have not been explored in prior studies.

3.2. *Spray dispersion and effect of fenders*

In Figure 8 we show two instantaneous snapshots of the TDS model with spray included. As in the case of the GCM, the smallest drops are most strongly transported by the flow, with a noticeable interaction between the vortex structures on the top of the rear wheel and the small droplets. Larger droplets injected at the bottom appear to travel in a nearly ballistic manner, with droplets injected from the back of the lead wheel generating finer spray upon collision with the rear wheel.

Finally, we consider the effect of fenders and fairings. In Figure 9 we show representative trajectories of massed particles having diameters of 1×10^{-4} and 1×10^{-5}m; it is clear that the trajectories of the small particles are largely unaffected by the fender while the larger particles appear to impact the inside surface of the fender. Based on the results observed using more detailed spray collision models in the TDS baseline and the GCM simulations, we anticipate that these events would generate fine mist that would then be transported into the wheel or vehicle wake. These preliminary simulations appear to

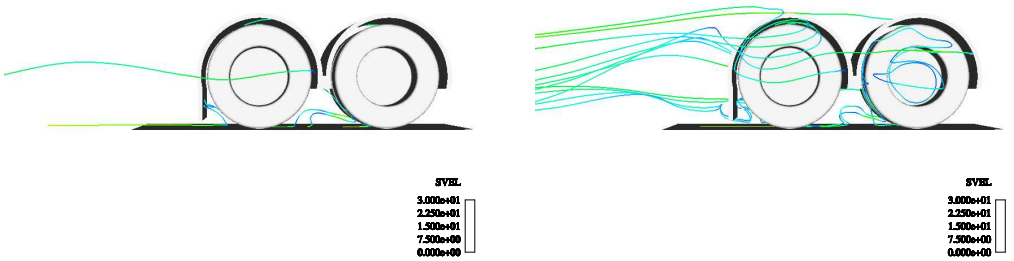

FIGURE 9. (Color) Particle trajectories in steady RANS flowfield about TDS with fender. Left: Particles with diameter 1×10^{-4}m; Right:diameter 1×10^{-5}m. Particle density is that of water. Note ineffectiveness of fender in constraining transport of small drops.

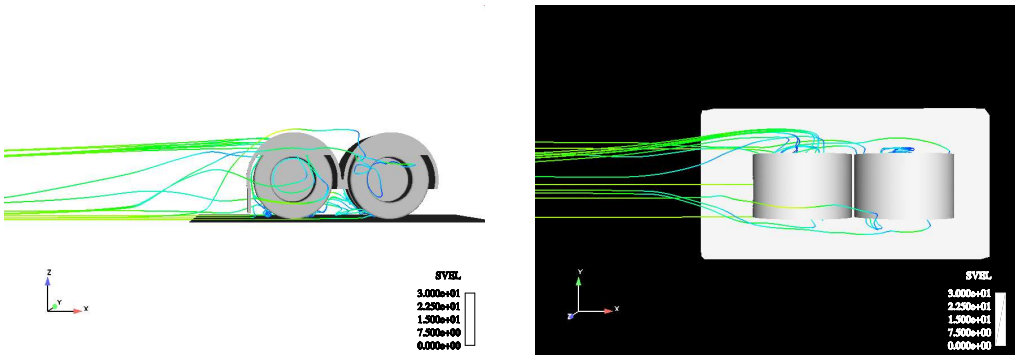

FIGURE 10. (Color) Particle trajectories in steady RANS flowfield about TDS with faired fender using particles with diameter 1×10^{-5}m. Left:View from faired side ; Right: View from top. Note the increased flow and particle transport to the non-faired (left) side of the assembly

agree with the aforementioned experimental studies that show that fenders appear to have little measurable impact on spray density or transport.

The effect of fairings appears to be marginal. In Figure 10, we present side views of the particle trajectories of the smallest (1×10^{-5}m) particles on the side with a fairing and from above. It is clear that the fairing appears to constrain the transport of small droplets, but with the opposite side of the wheel open, the flow and spray are preferentially pushed to the inside. This means that spray may actually be concentrated directly behind the vehicle while the spray to sides is minimized, making passing easier but at the same time making driving more dangerous for a motorist following the tractor-trailer. This finding may be consistent with that of Dumas & Lemay (2004) in which faired fenders improved the side line-of-sight opacity measurements. Since no opacity measurements were made directly behind the test tractor-trailer, it is unclear if the visibility loss due to spray was decreased for a following (as opposed to passing) motorist.

4. Conclusions and suggestions for future work

A preliminary investigation of spray transport in heavy vehicle and wheel wakes was completed using the commercial code StarCD. The empirical spray models included collision and aerodynamic breakup modes; the former was found to be of primary importance. The central findings of this study are:

• CFD codes and computational resources are now capable of of investigating the splash and spray problem

• Tandem dual wheel aerodynamics involve significant complexity and computational cost; the flow field is extremely unsteady and three-dimensional

• Preliminary spray calculations on wheel geometries indicate that small droplets interact strongly with the coherent structures in the wake and that fenders or fairings do not strongly affect spray transport

This first attempt at simulating spray dispersion in tractor-trailer or wheel wakes employed a number of simplifications and assumptions. Some important details that require further study are:

• Droplet sizes and velocities as well as injection points were assumed. The work of Fred Browand at USC will improve the specification of these considerably

• The breakup model for droplet-surface collisions is designed for gas in engine cylinders. An experimental study examining the breakup physics or simply to obtain the correct empirical coefficients for the model used would improve the accuracy

• The effect of crosswinds on devices is clearly important and is probably responsible for much of the apparently contradictory experimental data on spray reduction. This effect is straightforward but computationally expensive to obtain as the mesh resolution requirements are severe

• The most accurate method to simulate the combined splash and spray problem is to couple the free-surface type models required for splash with the Lagrangian particle-tracking type models used for spray; this coupling is quite difficult to implement accurately and requires efficient means of capturing breakup

• Unsteady RANS has well-known shortcomings for separated bluff-body wake flows; computationally efficient LES or hybrid RANS-LES models are necessary to improve to temporal accuracy and spatial resolution of vortical structures in the flow that are known to strongly affect particle dispersion

In closing, although considerable empiricism is still required, CFD makes it possible to complete controlled studies of the effectiveness of spray suppression devices and may make the intelligent design of such devices a reality.

5. Acknowledgments

Helpful conversations with and feedback on this manuscript from Rose McCallen, Kambiz Salari, Jason Ortega and Paul Castellucci is gratefully acknowledged. This work was performed under the auspices of the U.S. Department of Energy by the University of California, Lawrence Livermore National Laboratory under Contract No. W-7405-ENG-48. UCRL-TR-218205

REFERENCES

CD ADAPCO 2005 StarCD v.3.24, http://www.cd-adapco.com/products/STARCD/index.html.

ALLAN, J. & LILLEY, G. 1983 The reduction of water spray from heavy road vehicles. *Int. J. of Vehicle Design* **SP3**, 270–307.

APTE, S., MAHESH, K., MOIN, P. & OEFELEIN, J. 2003 Large-eddy simulation of swirling particle-laden flows in a coaxial-jet combustor. *Intl. J. Multiphase Flow* **29**, 1311–1331.

AXON, L., GARRY, K. & HOWELL, J. 1999 The influence of ground condition on the flow around a wheel located within a wheelhouse cavity. *Tech. Rep.* 1999-01-0806. SAE.

BAI, C., RUSCHE, H. & GOSMAN, A. 2002 Modeling of gasoline spray impingment. *Atomization and Sprays* **12**, 1–27.

Basara, B., Beader, D. & Przulj, V. 2000 Numerical simulation of the air flow around a rotating wheel. In *3rd MIRA International Vehicle Aerodynamics Conference*.

Blackburn, H., Mansour, N. & Cantwell, B. 1996 Topology of fine scale motions in turbulent channel flow. *J. Fluid Mech.* **310**, 269–292.

CEI 2005 Ensight v.8.07, http://www.ensight.com/products/ensight.html.

Crowe, C., Sommerfeld, M. & Tsuji, Y. 1998 *Multiphase flows with droplets and particles*. CRC Press.

Dubief, Y. & Delcayre, F. 2000 On coherent-vortex identification in turbulence. *J. Turbulence* **1**, 011.

Dumas, G. & Lemay, J. 2004 Splash and spray measurement and control: Recent progress in quebec. In *The Aerodynamics of Heavy Vehicles: Trucks, Buses and Trains* (ed. R. McCallen, F. Browand & J. Ross), *Lecture Notes in Applied and Computational Mechanics*, vol. 19, pp. 533–547. Springer.

Durbin, P. & Reif, B. P. 2003 *Statistical Theory and Modeling for turbulent flows*. Wiley.

Elofsson, P. & Bannister, M. 2002 Drag reduction mechanisms due to moving ground and wheel rotation in passenger cars. *Tech. Rep.* 2002-01-0531. SAE.

Goering, E. & Kramer, W. 1987*a* Improving the active and passive safety of commercial vehicles by lateral chassis fairings. *Automobiltech Zeitscrhift* **89**, 659–666, in German.

Goering, E. & Kramer, W. 1987*b* Lateral chassis fairings for commercial vehicles: An effective aid for the further improvement for aerodynamics, safety, and environmental acceptability. *Automobiltech Zeitscrhift* **89**, 481–488, in German.

Hedges, L., Travin, A. & Spalart, P. 2002 Detached-eddy simulations over a simplified landing gear. *ASME J. Fluids Eng.* **124**, 413–423.

Knowles, R., Saddington, A. & Knowles, K. 2002 On the near wake of rotating, 40%-scale champ car wheels. *Tech. Rep.* 2002-01-3293. SAE.

Manser, M., Koppa, R. & Mousley, P. 2003 Evaluation of splash and spray suppression devices on large trucks during wet weather. *Tech. Rep.*. AAA Foundation for Traffic Safety, www.aaafoundation.org.

Mears, A., Dominy, R. & Sims-Williams, D. 2002 The air flow about an exposed racing wheel. *Tech. Rep.* 2002-01-3290. SAE.

Menter, F. 1994 Two-equation eddy-viscosity turbulence models for engineering applications. *AIAA J.* **32**, 1598–1605.

NHTSA 2000 Update on the status of splash and spray suppression technology for large trucks. Report to Congress.

O.D.O.T. 2002 MCTD Form 2351A: Splash and Spray Suppressant Device Requirements, http://www.odot.state.or.us/forms/motcarr/2351a.pdf.

Pilch, M. & Erdman, C. 1987 Use of breakup time data and velocity history data to predict the maximum size of stable fragments for acceleration-induced breakup of a liquid drop. *Int.J.Multiphase Flow* **13** (6), 741–757.

Salari, K., Ortega, J. & Castellucci, P. 2004 Computational prediction of aerodynamic forces for a simplified integrated tractor-trailer geometry. *Tech. Rep.*. AIAA-2004-2253.

Sharc 2005 Harpoon v.1.49, http://www.sharc.co.uk.

Skea, A., Bullen, P. & Qiao, J. 2000 Cfd simulations and experimental measurements of the flow over a rotating wheel in a wheel arch. *Tech. Rep.* 2000-01-0487. SAE.

Waschle, A., Cyr, S., Kuthada, T. & Wiedemann, J. 2004 Flow around an isolated wheel - experimental and numerical comparison of two cfd codes. *Tech. Rep.* 2004-01-0445. SAE.

Weir, D., Strange, J. & Heffley, R. 1978 Reduction of adverse aerodynamic effects of large trucks: Vol. 1: Technical report. *Tech. Rep.* FHWA-RD-79-84, STI-TR-1093-01. Systems Technology, Inc., Interim Report to Federal Highway Administration.

Wilcox, D. 2002 *Turbulence Modeling for CFD*. DCW Industries.

Zdravkovich, M. 2003 *Flow around circular cylinders, Vol. 2: Applications*. Oxford University Press.